

Studies of Binary Layered CH₃OH/H₂O Ices Adsorbed on a Graphite Surface

Angela J. Wolff, Carolina Carlstedt, and Wendy A. Brown*

Department of Chemistry, University College London, 20 Gordon Street, London, WC1H 0AJ, United Kingdom

Received: November 8, 2006; In Final Form: February 6, 2007

Reflection absorption infrared spectroscopy (RAIRS) and temperature programmed desorption (TPD) have been used to investigate binary layered ice systems consisting of methanol deposited on top of various thicknesses of water ice, grown on an underlying graphite surface. RAIRS shows that there is no difference between the RAIR spectra recorded for pure ices and that recorded for the layered ices, suggesting that there is no discernible interaction between the layers during adsorption. However, annealing the ice layers leads to intermixing, as evidenced by a 50 cm⁻¹ downshift of the O–H stretching frequency of the mixed ice, compared to that expected from a simple combination of the pure water and pure methanol O–H stretching bands. TPD shows several new species when compared with TPD spectra for pure ices, confirming that mixing of the ice layers occurs on heating. A TPD peak that can be assigned to the trapping of methanol within the water ice is observed. TPD peaks for the desorption of monolayer and multilayer methanol are also observed.

Introduction

Methanol (CH₃OH) is one of the most abundant molecular species observed in the interstellar medium (ISM)¹ where it is usually found in the form of interstellar ices, frozen out on the surface of dust grains.² CH₃OH is typically observed within water (H₂O) rich ices and, where present, is often the most abundant molecule after H₂O.^{3–6} Its abundance in grain mantles is predicted to vary between 0.05 and 0.50 relative to H₂O,^{5,7} although it is generally considered that the lower abundance estimates are more accurate.⁷

Given the close association of CH₃OH with H₂O in the ISM, a detailed understanding of the adsorption of CH₃OH on, and its desorption from, the surface of ice-covered grains is vital to enable accurate modeling of the ISM and to explain the observed gas-phase abundances of CH₃OH and H₂O.⁸ The adsorption and desorption of ices is also important in cometary environments⁶ and in regions where shocks lead to sudden heating of the grains, and hence to desorption (followed by subsequent re-adsorption) of the ices.^{9–11} With this in mind, we have used reflection absorption infrared spectroscopy (RAIRS) and temperature-programmed desorption (TPD) to investigate the adsorption of CH₃OH on H₂O layers of various thicknesses adsorbed on a highly oriented pyrolytic graphite (HOPG) substrate held at around 97 K.

Dust grains in the ISM consist mainly of carbonaceous and siliceous material and are often covered in films of ice.² HOPG can therefore be considered as a suitable dust grain analogue and this surface has previously been used in investigations of H₂ formation on dust grains.^{12–15} The temperature in the ISM, where these ice-covered grains are found, is around 10–20 K. Although the experiments described here were not performed at this temperature, they still allow an understanding of the interaction of CH₃OH with layers of H₂O ice to be gained. The temperature of the ices found in comets and in shocked regions is often somewhat higher than that in the ISM, and can be as high as 100 K.

We have previously investigated the adsorption of pure CH₃OH¹⁶ and pure H₂O¹⁷ on the surface of HOPG. However,

combining studies of pure ices does not necessarily give reliable results when modeling the behavior of mixed ices. It is for this reason that we have performed detailed investigations of the adsorption and desorption of binary layered ices consisting of CH₃OH deposited on top of H₂O ice. H₂O ice is known to exist in a number of different phases depending on the temperature and deposition conditions.^{18–20} Previous studies have shown that H₂O ice grows as amorphous solid water (ASW) at deposition temperatures less than 135 K. ASW is therefore the dominant phase of the H₂O layers upon which CH₃OH is adsorbed in this work.

ASW has aroused much interest as it undergoes a structural transition that alters its porosity and surface area and can result in the trapping of volatile species.^{21–25} Collings and co-workers have shown, using TPD, that CO can be trapped within the pores of amorphous ice²⁴ and Bar-Nun and co-workers²² have highlighted the ability of ASW to trap Ar within a clathrate hydrate complex. Clathrate hydrates are crystalline regions of H₂O ice that enclose or engage small amounts of a guest molecule within the structure.²⁶ They are generally formed under high-pressure conditions and there is therefore some discussion about whether they will form in the ISM. TPD experiments of Collings and co-workers²⁷ have suggested that CH₃OH is too large to diffuse into the porous structure of H₂O ice, however, Blake and co-workers^{26,28,29} have suggested that CH₃OH can form a clathrate structure, albeit a slightly distorted version, described as a type II clathrate hydrate.

There are several previous studies of mixed CH₃OH and H₂O ices;^{6,26,27,30–33} however there are few previous studies of binary layered ice systems. Souda and co-workers performed a detailed study of CH₃OH and D₂O layers, in particular focusing on how layered structures of CH₃OH and D₂O intermix.^{34,35} They observed thermally induced isotope scrambling³⁵ and their studies showed that the two layers completely intermix above the glass transition temperature of D₂O/H₂O³⁴ at 136 K.

There have been a number of previous infrared studies of mixed CH₃OH and H₂O ices,^{36–38} sometimes with additional species such as CO and NH₃ within the mix.^{30,31} Although these previous studies focused on intimate mixtures, rather than the discrete layered structures described here, the work has em-

* Address correspondence to this author. E-mail w.a.brown@ucl.ac.uk.

phasized the importance of conducting infrared studies of complex H₂O dominated ices. In addition, there has been some suggestion in the literature that mixed polar ice mantles may undergo molecular segregation³⁹ to form layered structures, hence studying layered ices is of relevance to these systems.

Here we describe RAIRS and TPD investigations of the adsorption of CH₃OH on various thicknesses of ASW, grown on an underlying HOPG substrate at ~97 K. Three separate adsorbate systems were studied to explore the adsorption and desorption of CH₃OH as a function of the underlying H₂O multilayer thickness. Our previous studies of pure H₂O adsorption on HOPG¹⁷ showed that three-dimensional islands of H₂O began to form on the surface following an exposure of 1–2 L. Bare patches of HOPG were also present at this exposure. As a result, the adsorption of CH₃OH on H₂O ice films resulting from exposures of 2, 10, and 50 L, corresponding to thin, medium, and thick multilayers of H₂O ice, respectively, were investigated. These will be described as CH₃OH/H₂O(2 L), CH₃OH/H₂O(10 L), and CH₃OH/H₂O(50 L), where the number in parentheses represents the exposure used to create the underlying H₂O ice in the layered system.

Methodology

Experiments were performed in an ultrahigh vacuum (UHV) chamber that has a base pressure of $\leq 2 \times 10^{-10}$ mbar. The HOPG sample was purchased from Goodfellows Ltd. and was cleaved prior to installation in the UHV chamber, using the "Scotch Tape" method.⁴⁰ The sample was mounted on the end of a liquid nitrogen cooled cold finger and its temperature was monitored with an N-type thermocouple. Temperature control, during dosing and TPD experiments, was achieved via the use of a Eurotherm temperature controller coupled to Itools software. The sample was cleaned before each experiment by annealing at 500 K in UHV for 3 min. Sample cleanliness was confirmed by the absence of any desorption during TPD experiments performed with no dosage. Ices were grown in situ by exposing the cold HOPG surface, held at 97 K, to a stream of gas by back-filling the chamber through a high precision leak valve. All exposures are reported in Langmuir (L), where 1 L = 10⁻⁶ mbar s, and were recorded during dosing with a mass spectrometer. We are not able to make accurate measurements of surface coverage in these experiments, but we estimate that a 300 L dose results in an approximate ice thickness of around 6 nm.⁴¹ H₂O (distilled, deionized water) and CH₃OH (99.9%, Aristar-BDH) purities were checked with a quadrupole mass spectrometer before each experiment and during dosing.

RAIR spectra were recorded with a Mattson Instruments RS1 Research Series Fourier transform infrared spectrometer coupled to a liquid nitrogen cooled MCT detector. All spectra were taken at a resolution of 4 cm⁻¹ and are the result of the co-addition of 256 scans. In RAIRS experiments where the sample was heated, it was annealed to a predetermined temperature, held at this temperature for 3 min, and then cooled back down to the base temperature before a spectrum was recorded. TPD spectra were recorded with a Hiden Analytical HAL201 quadrupole mass spectrometer. All TPD spectra were recorded at a heating rate of 0.50 ± 0.01 K s⁻¹.

Results and Discussion

RAIRS Data. (A) *Adsorption.* Increasing exposures of CH₃OH were dosed onto an existing film of H₂O ice, grown on HOPG at 97 K, to form a layered ice structure. The deposition temperature of 97 K is well below the glass transition temperature of H₂O (136 K) and hence the H₂O ice formed is in the

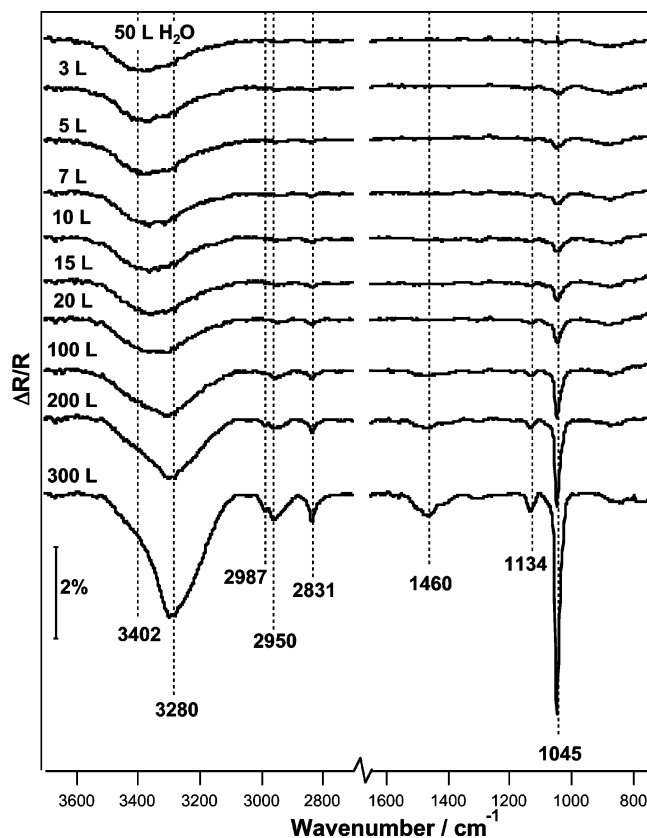


Figure 1. RAIR spectra recorded following the adsorption of increasing exposures of CH₃OH onto a 50 L layer of H₂O ice adsorbed on HOPG at 97 K. The top spectrum is that which is observed following an exposure of 50 L of H₂O. The total CH₃OH exposures are marked on the figure.

ASW phase. The phase of the H₂O ice film was confirmed by comparing the O–H stretching region of the pure H₂O RAIR spectrum with previous studies that have documented the crystalline/amorphous infrared fingerprint^{17,42,43} of H₂O ice. The RAIR spectra showed that, following an exposure of 50 L of H₂O, the main O–H peak produced is centered at 3392 cm⁻¹ with a low frequency shoulder at 3324 cm⁻¹. The appearance of the O–H stretching region of the pure H₂O ice films was characteristic of the formation of ASW.¹⁷

Figure 1 shows RAIR spectra of the CH₃OH/H₂O(50 L) system following the adsorption of increasing amounts of CH₃OH onto the H₂O ice film. The initial trace obtained, following the adsorption of 50 L of H₂O, shows the features expected for pure H₂O adsorbed on HOPG,¹⁷ namely a broad peak between 3050 and 3600 cm⁻¹, assigned to the O–H stretch. The other traces in Figure 1 show the effect of depositing increasing amounts of CH₃OH on top of the H₂O ice. With an initial 3 L exposure of CH₃OH an additional peak is observed in the spectrum at 1045 cm⁻¹. Increasing the exposure beyond 7 L results in the appearance of additional spectral features at 1134, 1460, 2831, 2950, and 2987 cm⁻¹. Figure 1 also shows that the appearance of the broad O–H feature between 3050 and 3600 cm⁻¹ noticeably changes when the CH₃OH exposure exceeds 20 L, with the growth of a new band centered on 3280 cm⁻¹ being observed. Exactly the same vibrational features are observed regardless of the thickness of the underlying H₂O layer. The only observed difference is a change in the shape of the O–H peak, with the CH₃OH/H₂O(50 L) system showing a broader O–H peak with a more pronounced high-frequency shoulder, corresponding to the greater H₂O contribution to the spectrum.

TABLE 1: The Assignment of the Vibrational Bands Observed for CH₃OH Adsorbed onto a 50 L Layer of H₂O Ice, Adsorbed on HOPG at 97 K, as Well as the Vibrational Frequencies for Physisorbed CH₃OH Adsorbed on HOPG¹⁶

band assignment	layered CH ₃ OH/H ₂ O(50 L)	multilayer CH ₃ OH (HOPG) ¹⁶
$\nu(\text{O}-\text{H})$	3402 ^a 3280	3260
$\nu_a(\text{CH}_3)$	2987 2950	2983 2956
$\nu_s(\text{CH}_3)$	2831	2833
$\delta_s(\text{CH}_3)$	1460	1468
$\rho(\text{CH}_3)$	1134	1132
$\nu(\text{C}-\text{O})$	1045	1045

^a The 3402 cm⁻¹ feature present in the layered system is attributed to the $\nu(\text{O}-\text{H})$ stretch of the H₂O layer.

The bands observed in the spectra shown in Figure 1 can all be assigned by comparison with the spectra previously obtained for pure H₂O¹⁷ and pure CH₃OH¹⁶ adsorbed on HOPG. Table 1 summarizes the assignments of the RAIRS bands observed in Figure 1, along with the previously reported vibrational bands observed for pure CH₃OH adsorbed on HOPG.¹⁶ If the complex O–H stretching region, which contains contributions from both the CH₃OH and H₂O present in the ice, is ignored then Figure 1 and Table 1 show that the CH₃OH vibrational bands have the same frequencies as those previously recorded for the formation of physisorbed CH₃OH multilayers on HOPG.¹⁶ This observation, and the fact that none of the vibrational bands seen in Figure 1 saturate as the exposure increases up to 300 L, indicates that physisorbed multilayers of CH₃OH are formed on top of the underlying layer of H₂O ice, as expected.

Any differences between the adsorption of CH₃OH on bare HOPG and that on an underlying H₂O ice film will only be observable for the lower CH₃OH exposures shown in Figure 1, where the CH₃OH is bonding directly to the H₂O ice film or to the bare HOPG surface. Once multilayers begin to grow there will be no observed difference between the spectra shown in Figure 1 and those previously recorded for CH₃OH adsorbed on a bare HOPG surface.¹⁶ However, even at low CH₃OH exposures, the spectra shown in Figure 1 are identical with those previously recorded for CH₃OH adsorption on bare HOPG. In addition, there are no observable differences between the RAIR spectra recorded for the CH₃OH/H₂O(2 L), CH₃OH/H₂O(10 L), and CH₃OH/H₂O(50 L) systems. These observations suggest that CH₃OH adsorption on bare HOPG cannot be distinguished from CH₃OH adsorption on a H₂O ice film. This is surprising, since it might be expected that CH₃OH would bond more strongly to H₂O than to HOPG. However, this fact is also confirmed by TPD (see later), which shows that it is not possible to distinguish separate desorption peaks for the adsorption of CH₃OH on HOPG and on the H₂O ice surface. This observation suggests that the intermolecular interactions between adjacent CH₃OH molecules are much more important in dictating CH₃OH adsorption on HOPG than the interactions between CH₃OH and the surface.

Confirmation of the observation that there is no noticeable change in the layered ices compared to the pure ice films comes from a closer inspection of the O–H stretching region between 3600 and 2600 cm⁻¹. Figure 2 compares the O–H stretching region for pure CH₃OH, pure H₂O, and the layered ice consisting of 50 L of CH₃OH deposited on top of 50 L of H₂O. Pure H₂O has a broad peak centered at 3390 cm⁻¹, pure CH₃OH has a peak at 3260 cm⁻¹, and the CH₃OH/H₂O(50 L) layered system gives a peak centered at 3330 cm⁻¹. Figure 2 shows that the RAIR spectrum resulting from the layered ice is well modeled

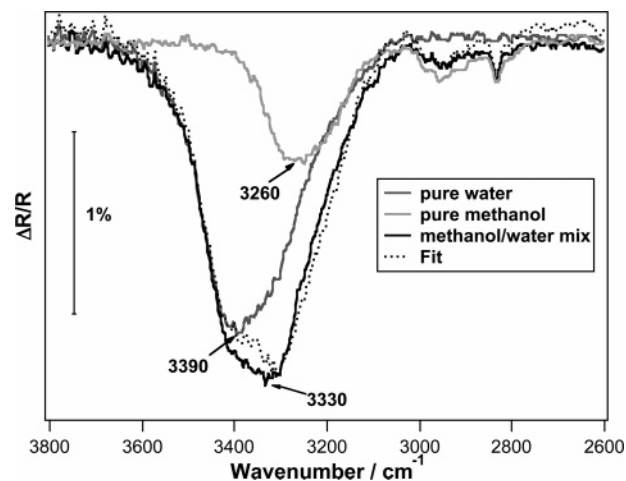


Figure 2. RAIR spectra for 50 L of pure H₂O, 50 L of pure CH₃OH, and 50 L of CH₃OH dosed onto an underlying 50 L H₂O layer, all deposited at 97 K. The fit generated by the addition of the pure CH₃OH and H₂O spectra is shown as a dashed line.

by a simple addition of the pure H₂O and pure CH₃OH spectra, suggesting that the sequential exposure of CH₃OH and H₂O onto the HOPG surface has caused little perturbation from the pure systems. Figure 2 implies that either the interactions between CH₃OH and H₂O are the same as those found in the pure ices or that the two species have remained as layers, without any mixing taking place during adsorption. RAIR spectra that result from the annealing of the sequentially deposited ice layers and TPD spectra for the same ice systems (shown later) do show evidence for mixing of the CH₃OH and H₂O layers. However, the RAIR spectra presented in Figure 2 show that this mixing only occurs as a result of the heating that occurs in the TPD experiment.

(B) *Annealing and Desorption of the Ice Layers.* Following adsorption, the desorption and annealing behavior of the three CH₃OH/H₂O layered ice systems was investigated. The behavior of all three ice systems was similar and hence the CH₃OH/H₂O(50 L) system has been chosen to illustrate the desorption behavior. Figure 3A shows RAIR spectra, focusing on the O–H stretching region, resulting from annealing the layered ice that results from depositing 50 L of CH₃OH on top of 50 L of H₂O ice. Figure 3B shows spectra focusing on the C–O stretching region, following annealing of the same ice. Figure 3A shows that there is little change to the O–H stretching region of the RAIR spectrum until the ice is annealed above 135 K. Annealing to 145 K causes the broad peak centered at 3361 cm⁻¹ to increase in amplitude and split into two peaks at 3361 and 3236 cm⁻¹. Annealing to 155 K causes the band at 3236 cm⁻¹ to increase in intensity and an additional low frequency shoulder at 3150 cm⁻¹ appears in the spectrum. This observed change in the O–H stretching region between 135 and 155 K can be assigned to the amorphous to crystalline phase transition of the H₂O ice film as previously observed for pure H₂O adsorbed on HOPG.¹⁷ Heating the ice above 155 K leads to a rapid loss in intensity of all of the bands seen in Figure 3A, indicating desorption of both the CH₃OH and H₂O layers. By 180 K, only a small peak at 3236 cm⁻¹ remains in the spectrum.

The peak at 3236 cm⁻¹ that remains in the spectrum, even after annealing to 180 K, has not previously been reported for either pure CH₃OH or pure H₂O ice adsorbed on HOPG. However, further detailed tests investigating the desorption of pure H₂O from the HOPG surface show that this peak can be assigned to the presence of pure H₂O. Integrating the area under the peaks shown in Figure 3A shows that the bands at 2943

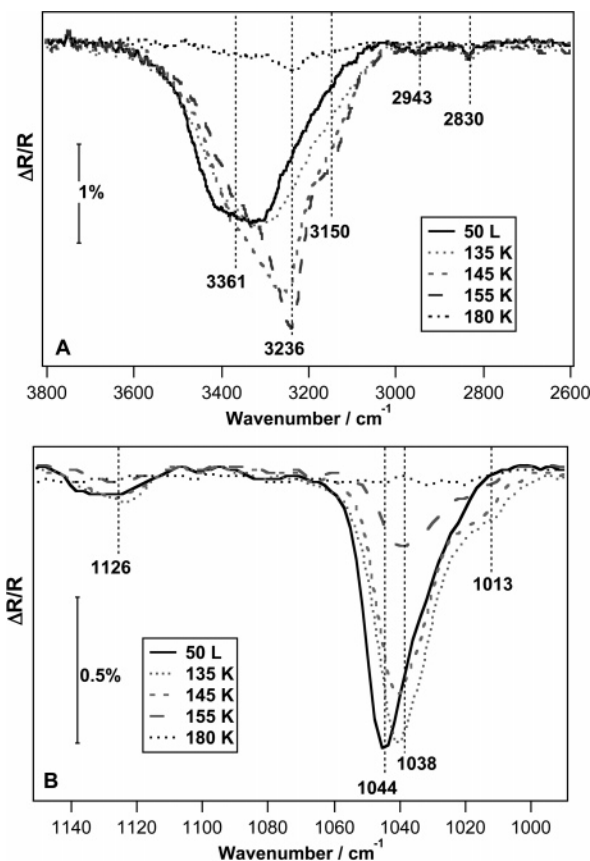


Figure 3. RAIR spectra showing the sequential heating of the layered ice formed by depositing 50 L of CH₃OH on top of 50 L of H₂O ice adsorbed on HOPG at 97 K: (A) the O–H stretching region between 2600 and 3800 cm⁻¹ and (B) the C–O stretching region between 980 and 1150 cm⁻¹.

and 2830 cm⁻¹, which can be assigned purely to CH₃OH, disappear from the spectrum around 170 K. This is higher than the desorption temperature of pure CH₃OH adsorbed on HOPG,¹⁶ which completely disappears from the RAIR spectrum by ~155 K. Interactions between the CH₃OH and H₂O that occur on heating therefore cause the CH₃OH to desorb at a higher temperature than observed for the pure ice system. The integrated area of the O–H stretch and the total integrated spectral area do not fall to zero until the annealing temperature is increased above 180 K, confirming the desorption of the H₂O layer at this temperature.

Figure 4 shows the results of an attempt to model the 3000–3600 cm⁻¹ RAIR spectrum that results from annealing the binary layered ice consisting of 50 L of CH₃OH deposited on top of 50 L of ASW to 155 K. The figure shows the fit achieved by the addition of pure H₂O and pure CH₃OH RAIR spectra for ices that have been annealed to 150 and 141 K, respectively. Note that the infrared spectrum resulting from the annealing of pure CH₃OH ice to 141 K, rather than 155 K, was used for the fit since pure CH₃OH adsorbed on HOPG would have desorbed almost completely by this temperature.¹⁶ As seen in Figure 4, the addition of these two peaks gives a very good fit to the shape of the layered ice spectrum, but the peak observed for the layered ice is ~50 cm⁻¹ lower in frequency when compared to the fitted spectrum. The inset to Figure 4 shows the fitted spectrum offset by 50 cm⁻¹ to confirm the quality of the fit. Moving the pure CH₃OH spectrum down by 50 cm⁻¹, before undertaking the addition, also produces a good fit without the need for a shift of the overall fitted spectrum. This suggests that the hydrogen bonding in the H₂O layer is not significantly

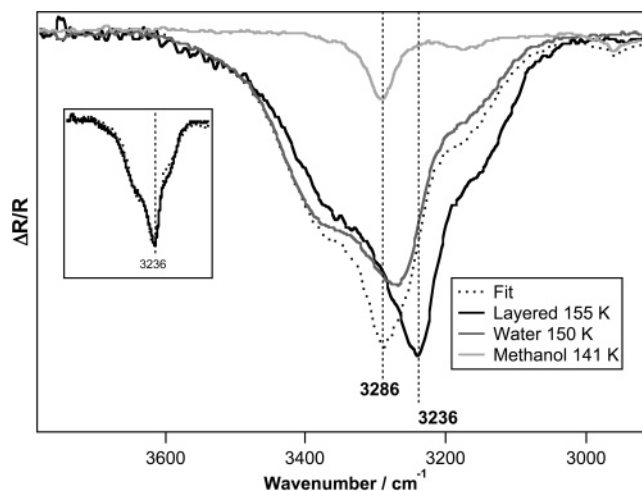


Figure 4. RAIR spectra for 50 L of pure H₂O annealed to 150 K, 50 L of pure CH₃OH annealed to 141 K, and 50 L of CH₃OH adsorbed on top of 50 L of H₂O ice annealed to 155 K, all grown on HOPG at 97 K. The fit generated by the addition of the pure CH₃OH and pure H₂O spectra is shown as a dotted line. The inset shows the fit shifted down by 50 cm⁻¹ to show the good overlap with the spectrum recorded for the layered CH₃OH/H₂O(50 L) ice annealed to 155 K.

disturbed by the CH₃OH molecules; however, the H₂O molecules clearly disrupt the bonding in the CH₃OH ice layer.

The observed downshift in frequency from that expected for a simple combination of the RAIR spectra for pure H₂O and pure CH₃OH, along with the increased desorption temperature of CH₃OH compared to that of pure CH₃OH,¹⁶ indicates that an interaction is occurring between the CH₃OH and the H₂O when the ice layers are annealed. This was not observed during adsorption at 97 K (see Figure 2) and therefore occurs as a direct result of the heating process. It is most likely that this interaction is caused by a temperature induced mixing of the H₂O and CH₃OH overlayers, as previously observed by Souda.³⁴ The downshift in the frequency of the O–H stretching mode suggests that the CH₃OH and H₂O form a hydrogen-bonded complex when the layers intermix. Strong hydrogen bonds act to weaken the O–H bond and therefore lower the frequency of the stretching vibration. They are also expected to increase the frequency of the O–H librational and bending modes, as these are both inhibited by hydrogen bonding.³⁸ However, these modes are not observed in the spectra reported here as they occur below the cutoff frequency of the MCT detector used in these experiments. In previous studies of matrix isolated CH₃OH:H₂O complexes, Bakkus and co-workers³⁶ observed a downshift of 20 cm⁻¹ in the O–H stretch when CH₃OH hydrogen bonds to O–H and acts as a proton donor. Hence the observed 50 cm⁻¹ downshift in the frequency of the O–H band for the layered ices, seen in Figure 4, can be attributed to the formation of a CH₃OH:H₂O complex.

Figure 3B shows the spectral region between 980 and 1150 cm⁻¹ (the C–O stretching region) for the spectra that result from annealing the binary layered ice consisting of 50 L of CH₃OH and 50 L of H₂O. Heating results in a decrease in the intensity of the C–O stretch at 1044 cm⁻¹ and a small downshift in frequency, with increasing annealing temperature. Immediately after heating, a small shoulder also appears at 1013 cm⁻¹. In contrast to the pure CH₃OH system,¹⁶ the C–O stretch at 1044 cm⁻¹ does not obviously split on heating, as would be expected for CH₃OH crystallization. However, it is likely that the shoulder at 1013 cm⁻¹ indicates the beginning of CH₃OH crystallization, as indicated by the frequency downshift of the 1044 cm⁻¹ C–O stretching mode. Results for the annealing of

pure CH₃OH adsorbed on HOPG¹⁶ indicate that crystallization is not observed for CH₃OH doses of less than 50 L, and therefore it is likely that the 50 L CH₃OH exposure in this study is just approaching the threshold coverage required for crystallization. Integration of the areas under the peaks shown in Figure 3B again shows that the bands assigned only to CH₃OH remain in the spectrum until ~ 170 K.

The annealing process was also repeated for each of the three ice systems, with a thicker CH₃OH overlayer formed by an exposure of 300 L of CH₃OH on top of the underlying H₂O layer. Unsurprisingly, the observed behavior is the same as that previously seen for the annealing of 300 L layers of pure CH₃OH adsorbed on HOPG.¹⁶ Both the O–H and C–O stretching bands are observed to split on annealing, providing evidence for crystallization of the CH₃OH ice. However, the desorption temperature of the CH₃OH is higher in the layered systems, compared to pure CH₃OH, as already noted.

TPD Data. TPD was also used to investigate the adsorption of various exposures of CH₃OH adsorbed on an underlying H₂O ice film. During TPD experiments, the desorption traces for masses 31, 32, and 18 were recorded simultaneously. Mass 31 is the major fragment detected by the mass spectrometer for CH₃OH and is therefore reported in preference to mass 32 throughout.

(A) *Water Desorption.* Figure 5 shows H₂O TPD spectra that result from the desorption of a binary layered ice system, grown on HOPG at 97 K, consisting of 2, 10, or 50 L of ASW with various thicknesses of CH₃OH dosed on top. In each trace (Figure 5A,B,C) the same amount of H₂O has been adsorbed, but the thickness of the CH₃OH layer is increasing in each case.

For the thinnest sublayer of H₂O ice, in the CH₃OH/H₂O(2 L) system, a single H₂O desorption peak is observed at 139 K for all CH₃OH exposures ≤ 50 L (Figure 5A). The integrated area under the H₂O TPD peaks seen in Figure 5A for the desorption of the 2 L H₂O layer also remains constant with increasing CH₃OH exposures ≤ 50 L. However, as the CH₃OH overlayer exposure increases to 100 L the H₂O TPD spectrum (Figure 5A) broadens and an additional peak is observed at 150 K. Following a 300 L exposure of the CH₃OH overlayer, the H₂O TPD spectrum in Figure 5A now shows a very sharp peak at 140 K with a shoulder at 143 K and a smaller peak at ~ 152 K. The integrated area underneath the H₂O TPD trace also increases following the deposition of 100 L or more of CH₃OH. The sharp H₂O desorption peak observed in Figure 5A coincides with the maximum desorption of CH₃OH (see later), also observed at 140 K.

Figure 5B shows H₂O desorption traces for the CH₃OH/H₂O(10 L) system. Following low exposures of CH₃OH onto the H₂O ice film, a single peak at 144 K is observed in the TPD spectrum. As the CH₃OH exposure increases, the H₂O desorption peak shifts up in temperature (see inset to Figure 5B) and, following a 300 L dose of CH₃OH, the peak temperature of the H₂O desorption is shifted to 155 K. As observed for the desorption of H₂O from the CH₃OH/H₂O(2 L) system, the H₂O desorption peak also broadens with increasing thickness of the CH₃OH overlayer. Despite this broadening, however, the total integrated area of the 10 L H₂O TPD peaks seen in Figure 5B is constant as a function of increasing CH₃OH exposure.

H₂O TPD spectra for the CH₃OH/H₂O(50 L) binary layered ice system also behave in a similar manner, as shown in Figure 5C. Again, for low exposures of CH₃OH a single H₂O desorption peak is recorded, which shifts up in temperature as the CH₃OH exposure increases (see inset to Figure 5C). In contrast to the CH₃OH/H₂O(10 L) system, the shift in peak

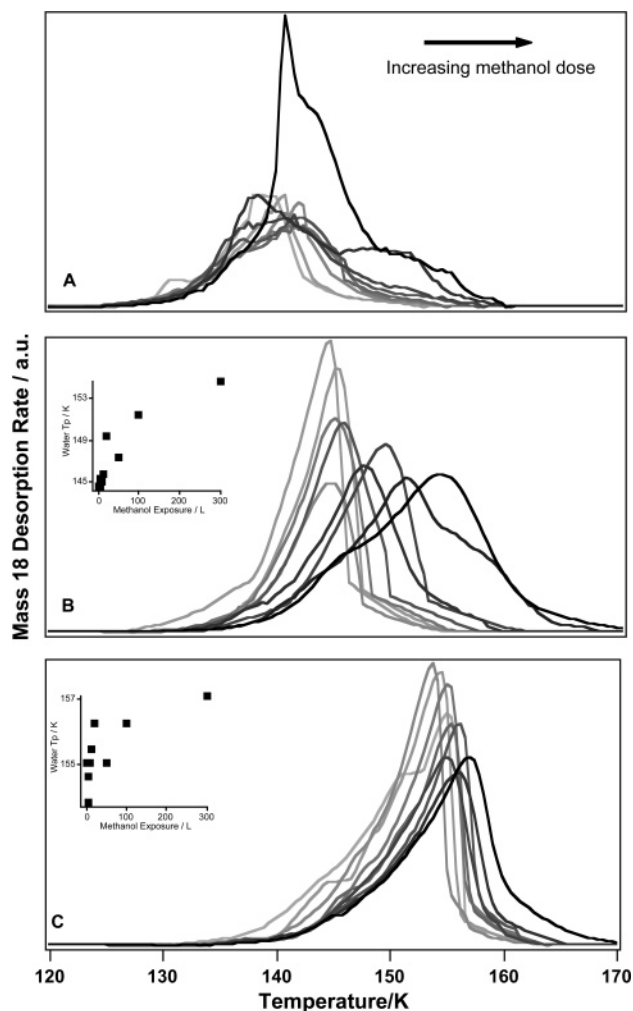


Figure 5. TPD traces showing the desorption of H₂O from CH₃OH/H₂O layered ices grown on HOPG at 97 K. The amount of CH₃OH adsorbed on the underlying H₂O ice film increases through the exposures of 3, 5, 7, 10, 15, 20, 50, 100, and 300 L. (A) The spectra resulting from dosing CH₃OH on top of a 2 L H₂O ice film; (B) the spectra resulting from dosing CH₃OH on top of a 10 L H₂O ice film; and (C) the spectra resulting from dosing CH₃OH on top of a 50 L H₂O ice film. The insets to parts B and C show the variation in the peak temperature of the H₂O desorption with increasing CH₃OH exposure.

temperature is fairly small with the peak initially being observed at 154 K and shifting up to 157 K following the adsorption of 300 L of CH₃OH. The H₂O desorption peak also broadens as the CH₃OH exposure increases, although this broadening is not as pronounced as that observed for the CH₃OH/H₂O(10 L) system. As for the CH₃OH/H₂O(10 L) system, the integrated area of the H₂O TPD peaks in Figure 5C is constant with increasing CH₃OH overlayer exposure. For both the 10 (Figure 5B) and 50 L (Figure 5C) H₂O traces, the sudden change observed in the H₂O desorption rate for the H₂O layers covered with thinner CH₃OH overlayers (left-hand traces in the figure) is most likely due to the crystallization of the underlying H₂O layer. The crystallization is masked at higher CH₃OH doses as it takes place before the H₂O desorption occurs, due to the increased desorption temperature of the H₂O layer with increasing CH₃OH overlayer thickness.

For each layered ice system, the H₂O exposure remains constant and hence the desorption temperature of the H₂O should also remain constant. The observed broadening and shifting of the H₂O TPD peaks in the CH₃OH/H₂O(10 L) and CH₃OH/H₂O(50 L) layered ices can be understood by comparing the

desorption temperature expected for pure H₂O ices, resulting from 10 and 50 L exposures on bare HOPG, with the desorption temperature of the overlying CH₃OH layer in each case. Figure 5 clearly shows that H₂O desorption is inhibited by the presence of thick overlayers of CH₃OH, which act to hold the H₂O in place on the surface. This results in a broadening of the H₂O desorption peak and an increasing peak temperature with increasing thickness of the CH₃OH overlayer. Due to the sequential nature of the dosing, the H₂O cannot desorb until the overlying CH₃OH has already desorbed. Hence, in cases where the CH₃OH desorption occurs around, or beyond, the pure H₂O desorption temperature, a delay will occur in the H₂O desorption resulting in a broadening of the TPD spectrum and a higher peak temperature. This is exactly what is observed for the CH₃OH/H₂O(10 L) system. A 10 L dose of pure H₂O desorbs from HOPG with a peak temperature of around 144 K. The desorption peak temperature of CH₃OH ice varies from around 130 to 145 K as the dose increases from 10 to 300 L, and hence as the CH₃OH dose increases there is a competition between the desorption of the H₂O and the CH₃OH that leads to a broadening and delay in the H₂O desorption. For the CH₃OH/H₂O(50 L) system, there is a much less pronounced effect on H₂O desorption as the CH₃OH overlayer thickness increases, since the desorption temperature of 50 L of pure H₂O is ~153 K, 10 K higher than the peak temperature of the desorption of a 300 L layer of CH₃OH (~144 K). Hence, in the CH₃OH/H₂O(50 L) system, the desorption of the H₂O layer is less affected by the presence of the CH₃OH overlayer.

It is clear from Figure 5 that the H₂O desorption observed for the CH₃OH/H₂O(2 L) system behaves somewhat differently compared to the other two layered ice systems. At low exposures of CH₃OH the H₂O desorption temperature remains approximately constant, but as the CH₃OH exposure increases above 100 L, the desorption temperature, peak shape, and integrated area of the 2 L H₂O desorption peak changes dramatically. The desorption temperature of a 2 L layer of pure H₂O is 139 K. The thicker CH₃OH overlayers therefore hold the underlying H₂O ice on the HOPG surface well past its expected desorption temperature. Hence by the time that a CH₃OH overlayer of 300 L has desorbed, with a peak desorption temperature of 144 K, the H₂O explodes from the surface at a rate that exceeds the pumping speed of the vacuum chamber, leading to a very sharp TPD peak and large integrated peak area.

(B) Methanol Desorption. TPD spectra following low exposures of CH₃OH adsorbed on 2, 10, and 50 L of H₂O ice adsorbed on HOPG at 97 K are shown in Figure 6. Figure 7 shows TPD spectra resulting from high exposures of CH₃OH on the same H₂O layers. For CH₃OH desorbing from the thinnest layer of H₂O ice (2 L), shown in Figures 6A and 7A, the TPD spectra are comprised of two peaks. At the lowest CH₃OH exposures, a single desorption peak is observed at 134 K. As the CH₃OH exposure is increased this peak shifts up in temperature to 136 K and appears to saturate between 7 and 10 L of CH₃OH exposure. For CH₃OH doses ≥ 7 L a second lower temperature desorption peak is also observed that shifts up in temperature with increasing CH₃OH dose, and grows to dominate the spectrum (Figure 7A). The peak does not saturate following a 300 L exposure of CH₃OH indicating, as already shown by RAIRS, that the CH₃OH is physisorbed on the underlying H₂O surface. Further evidence for the formation of physisorbed CH₃OH comes from a plot of the total integrated area of the TPD peaks seen in Figures 6 and 7 as a function of exposure (not shown) that shows a linear increase, that never saturates, with increasing CH₃OH dose. The TPD spectra for

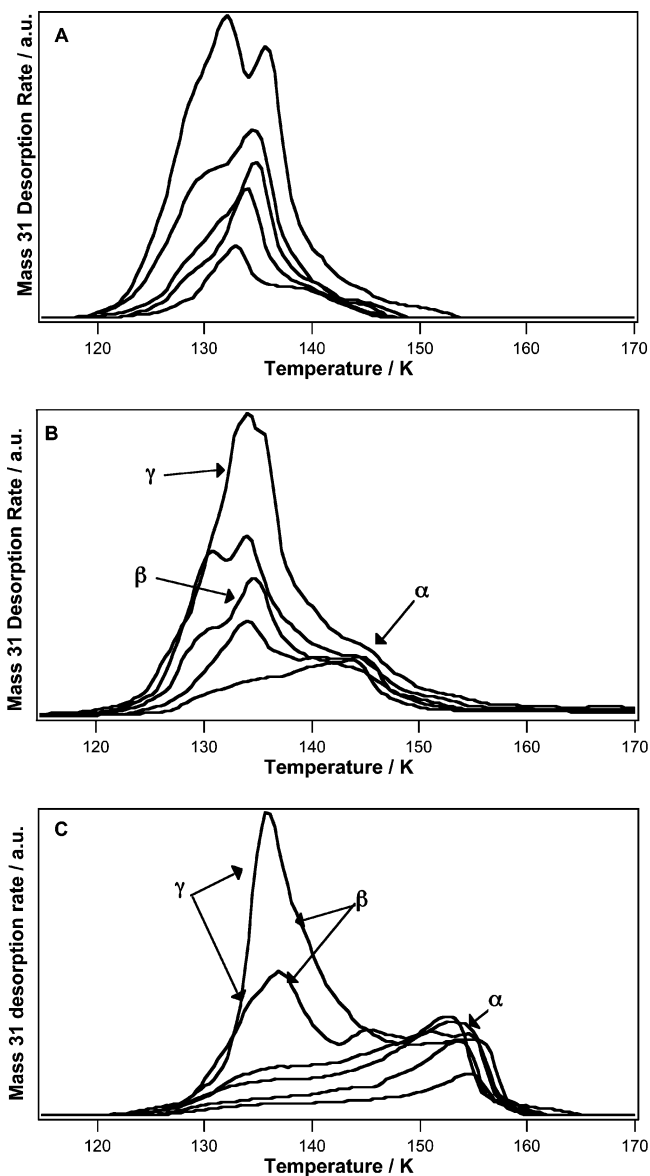


Figure 6. CH₃OH TPD spectra following low exposures of CH₃OH on (A) 2, (B) 10, and (C) 50 L of H₂O ice adsorbed on HOPG at 97 K. The spectra in part A and B follow CH₃OH exposures of 3, 5, 7, 10, and 15 L of CH₃OH on top of the underlying H₂O ice layer. Part C additionally shows the TPD spectrum resulting from a 20 L dose of CH₃OH.

the CH₃OH/H₂O(2 L) layered ice are essentially identical with those observed for the desorption of pure CH₃OH adsorbed on HOPG.¹⁶ The higher temperature peak, observed at low CH₃OH exposures, is therefore assigned to the formation of monolayer CH₃OH and the lower temperature peak that dominates the TPD spectra at high coverage is assigned to the desorption of multilayer CH₃OH.

TPD spectra for the desorption of CH₃OH deposited on thicker layers of H₂O ice (10 and 50 L) are more complex. Figure 6B shows a series of TPD spectra for increasing exposures of CH₃OH on 10 L H₂O ice. At very low CH₃OH exposures only a single high-temperature peak is observable at 145 K, labeled α . Increasing the exposure of CH₃OH does not lead to an increase in the intensity of this peak, suggesting that it has already saturated after only a 3 L CH₃OH dose. Instead, increasing the CH₃OH exposure leads to the appearance of a second lower temperature peak at 133 K, labeled β . At exposures of 7 L and above a third peak, labeled γ , appears as a low

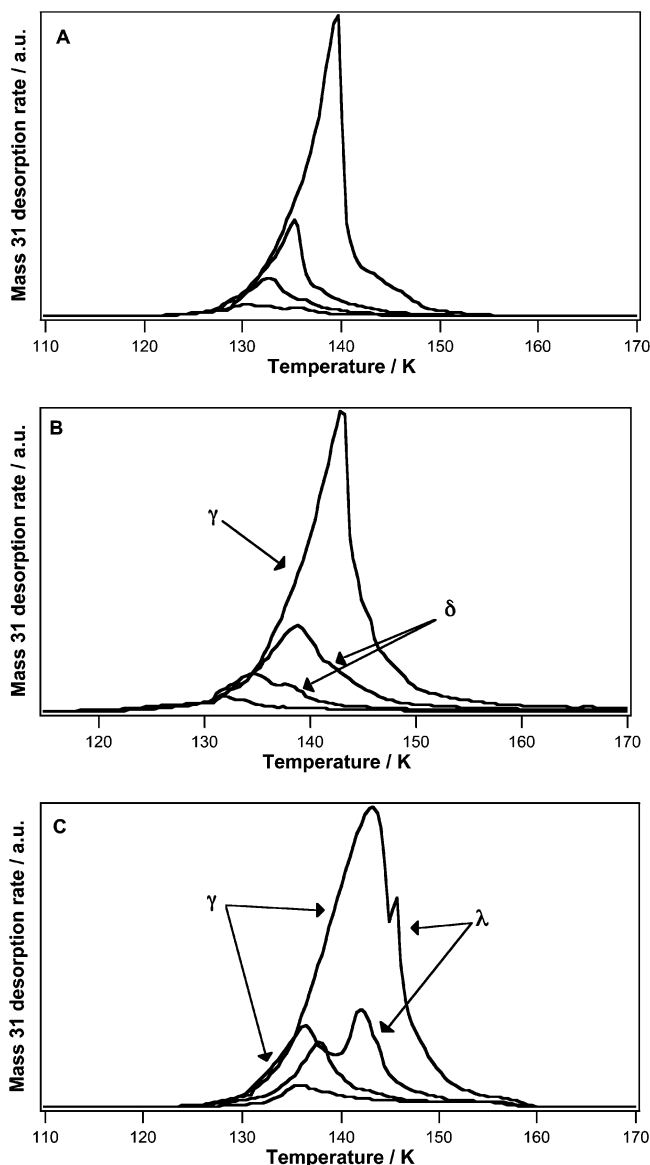


Figure 7. CH₃OH TPD spectra following high exposures of CH₃OH on (A) 2, (B) 10, and (C) 50 L of H₂O ice adsorbed on HOPG at 97 K. The spectra follow CH₃OH exposures of 20, 50, 100, and 300 L of CH₃OH on top of the underlying H₂O ice layer.

temperature shoulder on peak β . Increasing the CH₃OH exposure above 15 L (Figure 7B) leads to an increase in peak γ , which grows to dominate the spectrum. Peak γ does not saturate, and by 300 L this peak has reached a desorption temperature of 143 K (Figure 7B). At higher CH₃OH exposures (≥ 50 L) an additional high-temperature shoulder, labeled δ , is also observed at ca. 140–145 K.

Figure 6C shows TPD spectra for increasing doses of CH₃OH on an underlying 50 L layer of H₂O ice. At CH₃OH exposures below 5 L, a broad desorption peak is observed between 124 and 160 K. Within this broad feature there is a single high-temperature peak at 153 K, labeled α . Increasing the CH₃OH exposure up to 10 L results in a saturation of the intensity of the α peak and an increase in the intensity of the lower temperature part of the broad desorption trace, although there is still no well-defined TPD peak observed. Following a CH₃OH exposure of 15 L, three additional peaks can also be observed—a low-temperature peak labeled γ , a shoulder labeled β , and an additional peak at 145 K. Increasing the CH₃OH exposure beyond 15 L leads to the γ peak growing to dominate

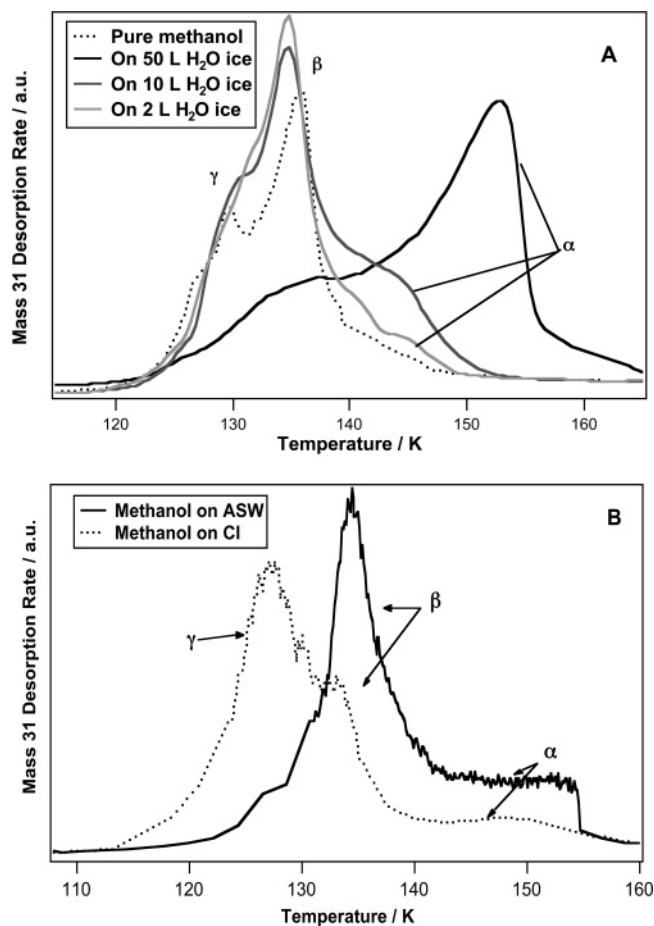


Figure 8. (A) TPD spectra for the desorption of 7 L exposures of CH₃OH adsorbed on a bare HOPG surface (dotted trace) and on various thicknesses of H₂O ice at 97 K. (B) TPD spectra showing the desorption of 15 L of CH₃OH adsorbed on a pre-adsorbed layer of amorphous solid water (ASW) and crystalline ice (CI) on an underlying HOPG surface at 97 K. In each case, the layers of H₂O ice resulted from a 10 L dose of H₂O.

the spectrum as seen in Figures 6C and 7C. Following a CH₃OH dose of 100 L, the γ peak splits into two clearly defined peaks. The low-temperature peak at 137 K is thought to be peak γ and the higher temperature peak is labeled λ . By 300 L the γ peak dominates the spectrum and the λ peak is still visible as a small peak at 146 K.

Assignment of the various TPD peaks seen for CH₃OH bonded to the H₂O layer can be made from a comparison of the TPD spectra observed in Figures 6 and 7 with those previously recorded for the desorption of CH₃OH from the bare HOPG surface.¹⁶ A comparison of low exposure (7 L) TPD spectra for CH₃OH adsorbed on bare HOPG and on H₂O layers of various thicknesses is shown in Figure 8A. From Figure 8A, it is clear that it is possible to assign peaks β and γ by comparison with the TPD spectra recorded for CH₃OH desorption from bare HOPG.¹⁶ Peak β is therefore assigned to the desorption of CH₃OH from the monolayer. If the H₂O and CH₃OH TPD traces are plotted on the same graph (Figure 9) it is clear that the β peak shares its leading edge with the H₂O desorption, suggesting that it desorbs as the H₂O first begins to sublime. This is consistent with the assignment of this peak to the desorption of monolayer CH₃OH adsorbed on top of the H₂O ice. Further evidence for the assignment of peak β to the formation of monolayer CH₃OH comes from a plot of the integrated area of each species in the TPD spectrum as a function of dose, as shown in Figure 10. The data in Figure 10 were

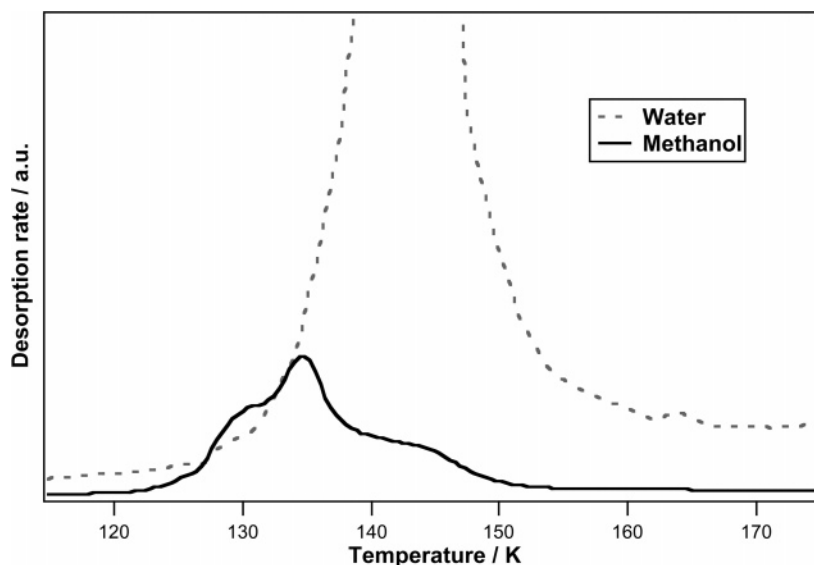


Figure 9. TPD spectra for 7 L of CH₃OH (solid line) deposited on an underlying layer of 10 L of H₂O ice on an HOPG surface at 97 K. The H₂O TPD trace (dotted line) is also shown for comparison. Note that there is not a considerably larger amount of H₂O on the surface compared to CH₃OH, as implied by the relative intensities of the CH₃OH and H₂O TPD peaks seen in this spectrum. The mass spectrometer response to H₂O is around 5 times larger than that to an equivalent amount of CH₃OH, hence the apparent observation that more H₂O is present than CH₃OH.

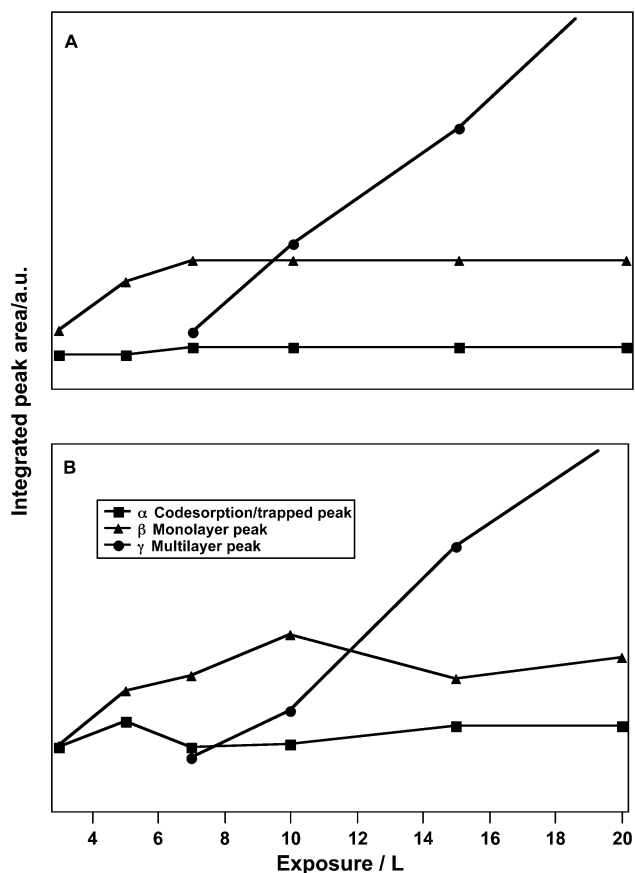


Figure 10. Curves showing the integrated area of the α , β , and γ TPD peaks shown in Figures 6 and 7 for (A) the CH₃OH/H₂O(2 L) and (B) the CH₃OH/H₂O(10 L) layered ice systems adsorbed on HOPG at 97 K.

produced by using a peak fitting package (SpXZeigR, Igor Pro, Wavemetrics Inc.) to separate out the individual contributions from the α , β , and γ peaks. Note that it was only possible to perform peak fits for CH₃OH dosed onto 2 and 10 L of H₂O ice as fits for the CH₃OH/H₂O(50 L) data were ambiguous. Figure 10 clearly shows that the area of the β peak saturates

with increasing exposure—a clear sign that this feature is due to the formation of a CH₃OH monolayer.

Surprisingly, it is not possible to distinguish between monolayer formation on the H₂O ice surface and monolayer formation on the HOPG surface. This was also the case for the RAIRS data, as discussed earlier. H₂O does not wet the HOPG surface, and instead has a tendency to form three-dimensional islands.⁴⁴ The result of this is that, following a 2 L exposure of H₂O (and maybe even following a 10 L H₂O exposure), bare patches of HOPG will be present. Hence CH₃OH will initially adsorb on both the bare HOPG and the H₂O islands. However, since only one monolayer CH₃OH TPD peak is seen in Figure 8A, CH₃OH bound to H₂O must have a similar desorption energy to CH₃OH directly adsorbed on HOPG. It is most likely that this is because the interactions between the CH₃OH molecules are more important than the interactions between the molecules and the surface.

Figure 8 shows that peak γ is also seen at the same temperature for the pure and layered ices and can therefore be assigned to desorption from within the multilayers of CH₃OH. As expected, the behavior of the multilayer TPD peak is identical for the three layered ice systems and for the pure CH₃OH ice. The δ peak, seen in the high-exposure TPD spectra for the CH₃OH/H₂O(10 L) system (Figure 7B), is thought to be due to the formation of crystalline CH₃OH and has been observed previously.^{16,45} RAIRS data, reported earlier, confirm that crystalline CH₃OH is formed when CH₃OH overlayers resulting from a dose of ≥ 50 L are heated above 130 K. The λ peak visible in the high exposure spectra of the CH₃OH/H₂O-(50 L) layered ice system (Figure 7C) is more difficult to assign. However, it is noted that the λ peak occurs at the same temperature as the amorphous to crystalline phase transition of H₂O (the amorphous to crystalline phase transition for pure H₂O adsorbed on HOPG occurs at 145–150 K)¹⁷ and it is therefore possible that the associated structural rearrangement leads to the release of CH₃OH molecules that have become trapped within the bulk of the H₂O ice as a result of heat induced mixing of the layers. This is a so-called “molecular volcano” peak and has previously been observed for co-deposited layers of CCl₄ and ASW.⁴⁶ A similar peak is also seen for the desorption of CH₃OH from co-deposited CH₃OH/H₂O ice systems.⁴⁷ The

observation of this peak clearly indicates that, as already suggested by the RAIRS data, mixing of the H₂O and CH₃OH layers occurs on heating.

The final feature observed in the TPD spectra in Figures 6 and 8 that still remains to be assigned is the α peak, observed following the lowest exposure of CH₃OH onto the underlying H₂O ice films. Figure 9 clearly shows that the α CH₃OH peak desorbs at the same time as the bulk of the H₂O ice. Peak α is a new peak that has not previously been observed for the desorption of CH₃OH from bare HOPG. It shows a desorption that is typical of trapped molecules and may represent CH₃OH trapped within the bulk of the H₂O ice. Previous work has suggested that CH₃OH forms a type II clathrate hydrate with H₂O ice;^{17,26} however, this seems unlikely in this case given that clathrate hydrates tend to form under high-pressure conditions. RAIRS data, reported earlier, have shown evidence for a strong hydrogen bonding interaction between the H₂O and the CH₃OH that occurs on annealing. It is therefore likely that this trapped CH₃OH species is hydrogen bonded to the H₂O that surrounds it, although the exact nature of the CH₃OH:H₂O complex that is formed is unknown.

RAIRS data have already shown that no interaction occurs between the H₂O and CH₃OH when adsorption occurs. Hence this trapping must occur as a result of the heating of the layered ice. Since the H₂O is deposited in the form of ASW, it will have a very porous and open structure. Any CH₃OH deposited onto this H₂O ice will therefore cover the surface and may also fill any holes within the ice structure. Previous work has shown that the pores of ASW, grown at 100 K, are too small for CHBr₃ to diffuse into⁴⁸ and therefore it is also likely that CH₃OH is too large to enter the pores of ASW, as previously indicated by Collings.²⁷ Heating of the ice will first lead to the desorption of monolayer CH₃OH, once the appropriate desorption temperature is reached. Heating the layered ice also leads to the conversion of ASW to crystalline ice, as evidenced by the O–H stretching region of the RAIR spectra. When this crystallization process takes place, some CH₃OH becomes trapped within the bulk of the H₂O ice, most likely at grain boundaries between the amorphous and crystalline ice which lead to holes being present in the annealed ice structure. This CH₃OH can only desorb when the bulk of the H₂O ice desorbs, as seen in Figure 9. The observed trapping leads to CH₃OH being retained on the surface for longer than expected when compared to CH₃OH adsorption on bare HOPG, as already noted in the RAIR spectra.

It is clear from Figure 8A that the three different layered ices show differences in the desorption temperature and the intensity of the saturated α peak. In fact, the percentage contribution of the α peak to the individual TPD curves increases with increasing thickness of the underlying H₂O layer. These differences can be understood by considering the differences in the structure of the H₂O ice film for the three layered ice systems. A 2 L exposure of H₂O ice will result in some three-dimensional structure to the ice layer, as H₂O tends to grow by island formation. However, bare patches of HOPG are also present and hence not much H₂O ice is available to trap the CH₃OH. Following a 10 L exposure of H₂O, the ice film has a greater volume, and so many more grain boundaries are formed on heating and hence more CH₃OH is trapped when crystallization occurs. Following a 50 L exposure of H₂O ice, considerable multilayer formation occurs, and the larger volume of the H₂O ice film leads to an increased amount of the trapped CH₃OH species that gives rise to peak α . Figure 8A shows that the peak temperature of the α feature apparently increases as

the thickness of the underlying H₂O layer increases. However, since the trapped CH₃OH desorbs only when the bulk H₂O ice desorbs then this temperature increase is most likely a function of the increasing desorption temperature of the underlying H₂O layer.

To confirm the assignment of peak α , a series of TPD experiments were performed for CH₃OH deposited on a sublayer of crystalline, rather than amorphous, H₂O ice (Figure 8B). The crystalline ice layer was formed by adsorbing H₂O on an HOPG surface held at an elevated temperature of 145 K. The surface was then cooled back to 97 K before dosing CH₃OH. The phase of the H₂O ice was confirmed by using RAIRS. Adsorption of CH₃OH on crystalline H₂O ice results in a less intense codesorption feature, peak α , and monolayer feature, peak β . As seen in Figure 8B, on the crystalline H₂O ice surface the multilayer feature, peak γ , is observed following a lower CH₃OH dose. These observations can be explained by considering the structure of the crystalline H₂O ice surface. Crystallization of the ice leads to a much denser structure, therefore reducing the surface area available for monolayer adsorption and reducing the entrapment of the CH₃OH. Hence the monolayer CH₃OH peak now saturates at a lower dose and multilayer growth is noted at lower coverages. A small α peak is still observed for CH₃OH adsorption on crystalline H₂O and can be explained by incomplete crystallization, as previously seen for H₂O adsorbed on bare HOPG.¹⁷ Notesco and Bar-Nun have also reported that a small amount of trapping can still take place within the crystalline phase of H₂O ice.³²

Previous work^{22,26,32} has observed similar trapping behavior for mixed CH₃OH/H₂O ices and the formation of type II clathrate hydrates has been proposed to explain the tendency of CH₃OH to remain on the surface until the H₂O has sublimed. Blake and co-workers²⁶ suggested the formation of the clathrate hydrate structure from around 130 K, when intermixing occurs. While we clearly see evidence of a strong interaction between the CH₃OH and the H₂O ice, we are unable to determine the exact nature of the trapped CH₃OH species without further structural investigations.

Conclusions

RAIRS investigations of the adsorption of CH₃OH onto an underlying H₂O ice film show that both CH₃OH and H₂O adsorb molecularly in a physisorbed state and that they remain isolated from each other in a layered morphology. RAIRS data also show that CH₃OH adsorption on an underlying layer of H₂O ice (grown in the form of ASW) cannot be distinguished from CH₃OH adsorption on bare HOPG, suggesting that the interactions between the individual CH₃OH molecules are more important than the interactions between the CH₃OH molecules and the surface. Annealing the layered ice leads to mixing of the CH₃OH and H₂O layers. TPD also shows evidence of mixing that occurs as a result of heating, with a TPD peak being observed that can be assigned to the trapping of CH₃OH within the H₂O ice structure. The TPD peak assigned to the trapped species increases in size as the thickness of the underlying H₂O layer increases, and is thought to arise due to the entrapment of CH₃OH at grain boundaries (or holes) that form in the H₂O ice as the amorphous to crystalline phase transition takes place. It is proposed that it is this trapped CH₃OH species that gives rise to the observed 50 cm⁻¹ shift in the O–H band observed in the RAIR spectra. TPD peaks are also seen for the desorption of monolayer and multilayer CH₃OH and, as seen with RAIRS, TPD cannot distinguish between monolayer CH₃OH desorbing from the H₂O surface and monolayer CH₃OH desorbing from

the bare HOPG surface. Additional TPD peaks are also observed that can be assigned to the formation, and desorption, of crystalline CH₃OH and also to the desorption of CH₃OH that occurs as the H₂O crystalline to hexagonal ice phase transition occurs.

The data reported here are of relevance to studies of the desorption of interstellar ices in areas such as comets, star-forming regions, and hot cores.^{8,49} Previous work has attempted to categorize the molecules found in interstellar ices according to their desorption characteristics.²⁷ These categories were then used to model the desorption of interstellar ices in hot core regions.⁸ CH₃OH was categorized as a “H₂O-like” species,²⁷ meaning that it shows desorption characteristics similar to those of H₂O. CH₃OH desorbing from a H₂O layer was not observed to trap within the structure of the H₂O ice and only the desorption of monolayer and multilayer CH₃OH was observed.²⁷ However, the peak assigned to the desorption of monolayer CH₃OH was coincident with the desorption of H₂O. Our results suggest that this monolayer peak should be reassigned to the desorption of CH₃OH trapped within the bulk of the H₂O ice. We are clearly able to distinguish the desorption of monolayer, multilayer, and trapped CH₃OH as shown by Figures 8 and 9. The apparent difference between our results and the previous results²⁷ can be explained by the different exposure ranges of the two experiments. Our experiments were performed over a wide range of CH₃OH exposures; however, the previous results only investigated the desorption of 5 L of CH₃OH adsorbed on the underlying H₂O ice surface. Hence it is clear that the previous classification of CH₃OH was limited by the exposure range used. Indeed, the authors of the previous work²⁷ pointed out that their study was an attempt at initial categorization of astrochemically relevant molecular species and that more detailed studies were needed to give a full understanding of the relevant adsorption systems. Our data have recently been used in astrochemical models to observe the effect of the different categorization of CH₃OH on the chemistry observed in star-forming regions.⁴¹

Acknowledgment. The UK EPSRC are gratefully acknowledged for a studentship for A.J.W. and also for an equipment and consumables grant (GR/S15273/01). This work forms part of the research currently being undertaken in the UCL center for cosmic chemistry and physics.

References and Notes

- (1) Garrod, R.; Park, I. H.; Cassell, P.; Herbst, E. *Faraday Discuss* **2006**, *133*, 51.
- (2) Williams, D. A. In *Dust and chemistry in astronomy*; Millar, T. J., Williams, D. A., Eds.; Institute of Physics: Bristol, UK, 1993.
- (3) Pontoppidan, K. M.; Dartois, E.; van Dishoeck, E. F.; Thi, W. F.; d'Hendecourt, L. *Astron. Astrophys.* **2003**, *404*, L17.
- (4) Pontoppidan, K. M.; van Dishoeck, E. F.; Dartois, E. *Astron. Astrophys.* **2004**, *426*, 925.
- (5) Sandford, S. A. *Meteorit. Planet. Sci.* **1996**, *31*, 449.
- (6) Sandford, S. A.; Allamandola, L. J. *Astrophys. J.* **1993**, *417*, 815.
- (7) Skinner, C. J.; Tielens, A. G. G. M.; Barlow, M. J.; Justtanont, K. *Astrophys. J.* **1992**, *399*, L79.
- (8) Viti, S.; Collings, M. P.; Dever, J. W.; McCoustra, M. R. S.; Williams, D. A. *Mon. Not. R. Astron. Soc.* **2004**, *354*, 1141.
- (9) Benedettini, M.; Yates, J. A.; Viti, S.; Codella, C. *Mon. Not. R. Astron. Soc.* **2006**, *370*, 229.
- (10) Hatchell, J.; Viti, S. *Astron. Astrophys.* **2002**, *381*, L33.
- (11) Viti, S.; Caselli, P.; Hartquist, T. W.; Williams, D. A. *Astron. Astrophys.* **2001**, *370*, 1017.
- (12) Katz, N.; Furman, I.; Biham, O.; Pirronello, V.; Vidali, G. *Astrophys. J.* **1999**, *522*, 305.
- (13) Perry, J. S. A.; Gingell, J. M.; Newson, K. A.; To, J.; Watanabe, N.; Price, S. D. *Meas. Sci. Technol.* **2002**, *13*, 1414.
- (14) Perry, J. S. A.; Price, S. D. *Astrophys. Space Sci.* **2003**, *285*, 769.
- (15) Pirronello, V.; Liu, C.; Roser, J. E.; Vidali, G. *Astron. Astrophys.* **1999**, *344*, 681.
- (16) Bolina, A. S.; Wolff, A. J.; Brown, W. A. *J. Chem. Phys.* **2005**, *122*, 044713.
- (17) Bolina, A. S.; Wolff, A. J.; Brown, W. A. *J. Phys. Chem. B* **2005**, *109*, 16836.
- (18) Backus, E. H. G.; Grecea, M. L.; Kleyn, A. W.; Bonn, M. *Phys. Rev. Lett.* **2004**, *92*, 236101.
- (19) Mayer, E.; Pletzer, R. *Nature* **1986**, *319*, 298.
- (20) Stevenson, K. P.; Gimmel, G. A.; Dohnalek, Z.; Smith, R. S.; Kay, B. D. *Science* **1999**, *283*, 1505.
- (21) Ayotte, P.; Smith, R. S.; Stevenson, K. P.; Dohnalek, Z.; Kimmel, G. A.; Kay, B. D. *J. Geophys. Res. [Planets]* **2001**, *106*, 33387.
- (22) Bar-Nun, A.; Dror, J.; Kochavi, E.; Laufer, D. *Phys. Rev. B* **1987**, *35*, 2427.
- (23) Bar-Nun, A.; Kleinfeld, I.; Kochavi, E. *Phys. Rev. B* **1988**, *38*, 7749.
- (24) Collings, M. P.; Dever, J. W.; Fraser, H. J.; McCoustra, M. R. S. *Astrophys. Space Sci.* **2003**, *285*, 633.
- (25) Jenniskens, P.; Blake, D. F. *Science* **1994**, *265*, 753.
- (26) Blake, D. F.; Allamandola, L. J.; Sandford, S. A.; Huggins, D.; Freund, F. *Science* **1991**, *254*, 548.
- (27) Collings, M. P.; Anderson, M. A.; Chen, R.; Dever, J. W.; Viti, S.; Williams, D. A.; McCoustra, M. R. S. *Mon. Not. R. Astron. Soc.* **2004**, *354*, 1133.
- (28) Blake, D. F.; Allamandola, L. J.; Freund, F.; Sandford, S. A.; Huggins, D. *IAU Symp.* **1992**, *150*, 437.
- (29) Blake, D. F.; Allamandola, L. J.; Sandford, S. A.; Freund, F. *Meteoritics* **1991**, *26*, 319.
- (30) Allamandola, L. J.; Sandford, S. A.; Valero, G. J. *Icarus* **1988**, *76*, 225.
- (31) Ehrenfreund, P.; Kerkhof, O.; Schutte, W. A.; Boogert, A. C. A.; Gerakines, P. A.; Dartois, E.; d'Hendecourt, L.; Tielens, A. G. G. M.; van Dishoeck, E. F.; Whittet, D. C. B. *Astron. Astrophys.* **1999**, *350*, 240.
- (32) Notesco, G.; Bar-Nun, A. *Icarus* **1997**, *126*, 336.
- (33) Notesco, G.; Bar-Nun, A. *Icarus* **2000**, *148*, 456.
- (34) Souda, R. *Phys. Rev. Lett.* **2004**, *93*, art no. 235502.
- (35) Souda, R.; Kawanowa, H.; Kondo, M.; Gotoh, Y. *J. Chem. Phys.* **2003**, *119*, 6194.
- (36) Bakkas, N.; Bouteiller, Y.; Loutellier, A.; Perchard, J. P.; Racine, S. *J. Chem. Phys.* **1993**, *99*, 3335.
- (37) Bakkas, N.; Bouteiller, Y.; Loutellier, A.; Perchard, J. P.; Racine, S. *Chem. Phys. Lett.* **1995**, *232*, 90.
- (38) Tielens, A. G. G. M.; Hagen, W.; Greenberg, J. M. *J. Phys. Chem.* **1983**, *87*, 4220.
- (39) Ehrenfreund, P.; Dartois, E.; Demyk, K.; d'Hendecourt, L. *Astron. Astrophys.* **1998**, *339*, L17.
- (40) Wiesendanger, R.; Eng, L.; Hidber, H. R.; Oelhafen, P.; Rosenthaler, L.; Stauffer, U.; Guntherodt, H. J. *Surf. Sci.* **1987**, *189*, 24.
- (41) Brown, W. A.; Viti, S.; Wolff, A. J.; Bolina, A. S. *Faraday Discuss* **2006**, *133*, 113.
- (42) Bensebaa, F.; Ellis, T. H. *Prog. Surf. Sci.* **1995**, *50*, 173.
- (43) Grecea, M. L.; Backus, E. H. G.; Riedmuller, B.; Eichler, A.; Kleyn, A. W.; Bonn, M. *J. Phys. Chem. B* **2004**, *108*, 12575.
- (44) Lofgren, P.; Ahlstrom, P.; Lausma, J.; Kasemo, B.; Chakarov, D. *Langmuir* **2003**, *19*, 265.
- (45) Pratt, S. J.; Escott, D. K.; King, D. A. *J. Chem. Phys.* **2003**, *119*, 10867.
- (46) Smith, R. S.; Huang, C.; Wong, E. K. L.; Kay, B. D. *Phys. Rev. Lett.* **1997**, *79*, 909.
- (47) Wolff, A. J.; Brown, W. A. In preparation.
- (48) Grecea, M. L.; Backus, E. H. G.; Kleyn, A. W.; Bonn, M. *Surf. Sci.* **2006**, *600*, 3337.
- (49) Williams, D. A. *Faraday Discuss* **1998**, *109*, 1.